Hindawi
International Journal of Aerospace Engineering
Volume 2022, Article ID 4481553, 14 pages
https://doi.org/10.1155/2022/4481553

Research Article

Reconfiguration Control Design of UAV against Actuator Faults Based on Control Allocation Method

Yuwei Cui, Aijun Li, Biao Duan, and Shabbir Wasif

School of Automation, Northwestern Polytechnical University, Xi'an Shaanxi 710072, China

Correspondence should be addressed to Yuwei Cui; cuiyuwei0505@mail.nwpu.edu.cn

Received 30 November 2021; Revised 5 April 2022; Accepted 11 May 2022; Published 28 May 2022

Academic Editor: Adel Ghenaiet

The paper concentrates on the problem of fault-tolerant control of UAV against actuator faults from the perspective of flight control system architecture. Using backstepping control method and inverse optimization theory, the design of backstepping optimal control law was constructed. Based on the fault monitoring mechanism of vehicle management computer in the distributed flight control and control allocation system, a fault-tolerant control design method was established in the case of multiple failure modes of the actuators, which compensates the influence caused by the failures. Finally, the effectiveness of the proposed strategy was verified by numerical simulation.

1. Introduction

In recent years, XQ-58A "Valkyrie" developed by the United States has started to verify its combat technology with manned fighters F-15X and F-35. While emphasizing joint operations, it also puts forward low-cost development requirements. This medium-size UAV with low-cost attritable aircraft technology (LCAAT) is more affordable than the X47B stealth UAV. In 2020, Russia demonstrated a high-speed, unmanned loyal wingman, named "Thunder". Similar to XQ-58A, it is capable of partnering with manned fighters and serving as a wingman in a front-line attack and detecting and destroying enemy and air defense targets, as discussed elsewhere [1–3].

With the worldwide research and development of all kinds of unmanned systems, the application of manned/unmanned aerial vehicles and unmanned swarm systems has been promoted. Unmanned systems are no longer synonymous with low cost and high risk but increasingly emphasize the following two aspects of technical requirements:

(i) Low cost and affordable economic cost

(ii) High fault tolerance and affordable security risks

For the fighter or large reconnaissance and combat UAVs, its cost can be increased. Therefore, the architecture of multiredundant hardware design is often used to improve the fault-tolerant ability of the entire aircraft system, especially for the flight control system with high safety and reliability. However, for consumable and low-cost unmanned systems such as loyal wingman, the architecture based on redundant hardware design brings high cost, large volume, large weight, and small load, which is often not acceptable. However, it is still expected to minimize the impact of failure, that is, to have higher fault tolerance.

There are many fault diagnosis and fault-tolerant control methods for sensors and actuators of flight control system. As early as 1990, as discussed by Professor Frank [4], international authority on fault diagnosis of control system divided fault diagnosis methods into three categories: analytical model-based methods, signal process-based methods, and knowledge-based methods, which have been accepted by many scholars [5, 6].

For the application of UAV flight control system, model-based fault detection, isolation, and adjustment methods can be used to reconstruct low redundancy/no redundancy signals for sensor faults, and the fault tolerance problem of

sensor signals can be solved by means of analytical redundancy, as discussed elsewhere [7–11].

But when the faults occur in the aircraft surface because of actuators, the detection and isolation method based on model cannot work, and it must be reconstructed through the control compensation of other surfaces to achieve fault tolerance. At present, many scholars have proposed adaptive control algorithms to solve various adaptive control problems in the case of surface failure, so as to achieve flight control, but the real-time performance of these algorithms is generally doubted, and a large number of algorithms need accurate mathematical models [12–15].

At present, the fault tolerant control towards actuator's faults is based on the results of fault detection [16]. Firstly, the faulty actuator should be isolated to avoid its fault spreading. Then, by adjusting the parameters of the controller or changing the structure of the controller, the stability and control performance of the system can be guaranteed. However, this method must be offline calculation of control law parameters required under various faults, and these parameters are stored in the flight control computer in advance. During the flight, according to the fault information obtained by fault detection, the matched control law parameters are selected to obtain the reconstructed flight control law. Since the parameters of the readjusted control law are designed off-line, the reconstructed flight control law can only tolerate the fault modes considered in advance, which limits the scalability of this method.

At the same time, we consider the possible failure modes of UAV actuators. At present, for small and medium-sized UAVs, electric actuators are basically used as the driving mechanism; and for large UAVs, with the continuous maturity of high-power electric actuators, the trend of replacing hydraulic actuators is also accelerating, due to the maintenance, pipeline, weight, leakage, and other problems caused by hydraulic actuators. Consider that there are two main failure modes of the electric actuators: nonoutput force and the output shaft stuck. From the perspective of surface control, the influence of the former is relatively small. And the most important thing is to realize fault detection, so that the fault can be found quickly. The second failure mode is trickier because it introduces additional unwanted moments that need to be balanced first in flight control.

In view of the multiple failure modes of UAV actuators, the strategy proposed in the paper adopts backstepping optimal control law and reconfiguration design based on a control allocation method to compensate the influence of faulty actuators, so as to achieve the goal of fault-tolerant control. The main contributions of the research are summarized as follows:

(1) Different from the adaptive control method, as referred to References [12–15], based on the optimal control law and the fault diagnosis result, control allocation methods carry out the mode switch. It does not need to carry out complex online calculation through the optimization algorithm, so it will not affect the real-time performance

(2) Compared with constructing off-line databases and adjusting the parameters or structure of controller, the reconfiguration control methods based on control allocation can compensate the influence of fault surfaces without adjusting the control law, thus extending its application scope

(3) More importantly, the paper presents a systematic solution, not just for the control algorithms. Through the modular control structure, the fault detection, control law, and control allocation algorithm are organically integrated, and a relatively comprehensive solution is proposed for the reconfiguration control against actuator faults

2. System Description and Preliminaries

A UAV adopts a conventional layout, and the independently controlled surfaces include the following: left fully moving elevator, right fully moving elevator, aileron, and V-shaped rudder. Because the left and right fully moving elevator can be controlled independently; that is to say, in addition to the pitching moment produced by the same deflection, the rolling moment can also be produced by the differential deflection, which provides additional control moment in the lateral direction. At the same time, the application of V-shaped rudder also provides a supplement for the generation of pitching moment. Therefore, the characteristics of multicontrol surfaces of the UAV provide conditions for the compensation control of actuators faults.

Firstly, the aircraft attitude dynamic equation in the body axial coordinate system is as follows:

$$\begin{bmatrix} \dot{\mu} \\ \dot{\alpha} \\ \dot{\beta} \end{bmatrix} = \begin{bmatrix} \dfrac{\cos\alpha}{\cos\beta} & 0 & \dfrac{\sin\alpha}{\cos\beta} \\ -\cos\alpha\tan\beta & 1 & -\sin\alpha\tan\beta \\ \sin\alpha & 0 & -\cos\alpha \end{bmatrix} \begin{bmatrix} p \\ q \\ r \end{bmatrix} + \begin{bmatrix} F_{\mu}(X) \\ F_{\alpha}(X) \\ F_{\beta}(X) \end{bmatrix}, \tag{1}$$

where α, β, and μ are, respectively, the angle of attack, sideslip angle, and roll angle and p, q, and r are, respectively, the pitch angle rate, yaw angle, rate and roll angle rate.

$$\begin{aligned} F_{\mu}(X) = {} & \frac{\sin\beta\cos\mu}{mV\cos\beta}\left(-D\sin\beta\sin\mu + L\cos\mu\right. \\ & \left. - Y\cos\beta\sin\mu - F_{\gamma t} - mg\cos\gamma\right) \\ & + \frac{\tan\gamma + \tan\beta\sin\mu}{mV}\left(D\sin\beta\cos\mu + L\sin\mu\right. \\ & \left. + Y\cos\beta\cos\mu + F_{\chi t}\right), \end{aligned}$$

$$\begin{aligned} F_{\alpha}(X) = {} & -\frac{\cos\mu}{mV\cos\beta}\left(-D\sin\beta\sin\mu + L\cos\mu\right. \\ & \left. - Y\cos\beta\sin\mu - F_{\gamma t} - mg\cos\gamma\right) + \frac{\sin\mu}{mV\cos\beta} \\ & \cdot \left(D\sin\beta\cos\mu + L\sin\mu + Y\cos\beta\cos\mu + F_{\chi t}\right), \end{aligned}$$

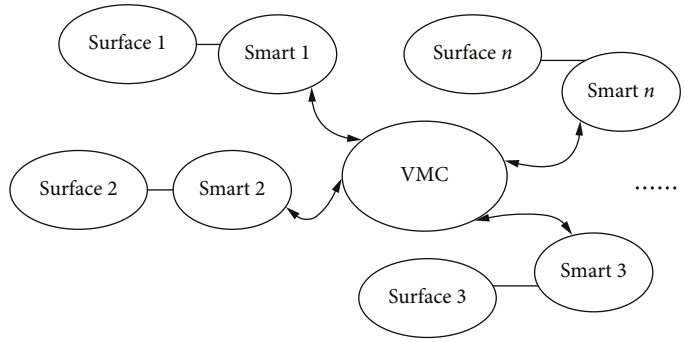

Figure 1: Distributed flight control system architecture.

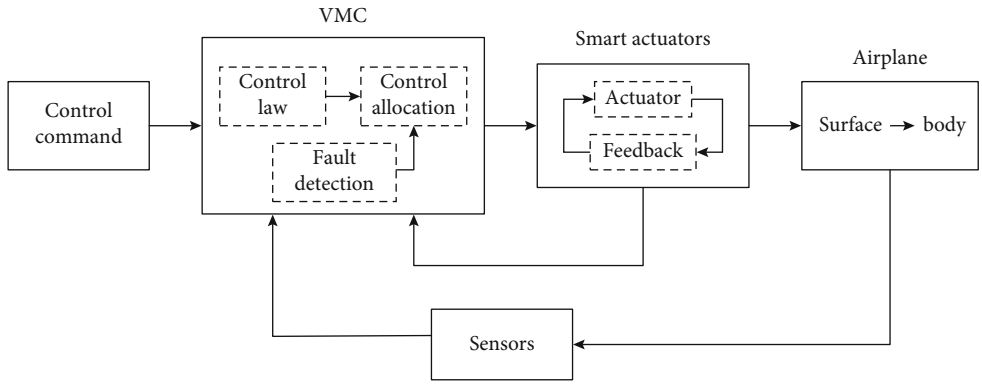

Figure 2: Reconfiguration control block diagram based on control allocation method.

$$F_\beta(X) = -\frac{\sin\mu}{mV}(-D\sin\beta\sin\mu + L\cos\mu - Y\cos\beta\sin\mu - F_{\gamma t} - mg\cos\gamma) + \frac{\cos\mu}{mV}(D\sin\beta\cos\mu + L\sin\mu + Y\cos\beta\cos\mu + F_{\chi t}),$$

$$F_{\chi t} = T\cdot dT\cdot(-\sin\mu\cos\alpha\sin\beta - \cos\mu\sin\alpha),$$

$$F_{\gamma t} = T\cdot dT\cdot(-\sin\mu\cos\alpha\sin\beta - \cos\mu\sin\alpha), \quad (2)$$

where m is mass, V is flight speed, γ is flight path angle, T is engine thrust, dT is thrust coefficient, and D, L, and Y are resistance force, lift force, and lateral force, respectively, as described below.

$$D = \bar{q}\cdot S\cdot c_d,$$
$$L = \bar{q}\cdot S\cdot c_l, \quad (3)$$
$$Y = \bar{q}\cdot S\cdot c_y,$$

where S is wing area, $\bar{q}$ is kinetic pressure, and c_d, c_l, and c_y are drag coefficient, lift coefficient, and lateral force coefficient, respectively.

Remark 1. The flight control system architecture of UAV can support the integrated design of actuator fault detection and flight control law. The following distributed system architecture in Figure 1 can be adopted [17–19]. The integrated VMC (vehicle management computer) realizes the fault detection of actuators, the calculation of flight control law, and the calculation of control allocation algorithm and finally forms the control instruction for each surface and transmits them to the SMART actuator located near the surface.

Remark 2. As shown in Figure 2, the integrated VMC will perform the fault detection, flight control law, and control allocation algorithm continually during the whole flight mission. The distributed system architecture, depending on the integrated design of VMC, can realize the reconfiguration control based on the control allocation method more conveniently, without affecting the servo control of the back-end actuator control loop in SMART. Meanwhile, it can be seen that after the introduction of control allocation module, the design of control law module in VMC does not need to be changed when some of actuators are faulty, which provides convenience for its application.

Remark 3. The fault detection toward actuators' fault modes needs to be added in the fault detection module of VMC. That is, the fault detection module can obtain all the data related to actuators fault modes, such as actuator position, motor HALL speed, and clutch drive current. Based on this, VMC can detect the failures of actuators. For example, when the motor HALL speed is high and the position of the actuator does not change, it can be considered that the actuator's output shaft is stuck at this time. When the clutch drive current is large, then the current control command of the motor

is cut off, and at this time, the actuator is in a state of non-output force. The paper does not make a comprehensive study of the specific fault detection strategy, only as the input conditions of the research.

3. Backstepping Optimal Controller Design

As we all know, the design of backstepping control law only considers the stability and convergence of the system and does not consider the optimal performance of the system [20, 21]. For the optimal control of the system, it is usually to find an admissible control with a given performance index, and the target functional takes the minimum value. This kind of problem ultimately comes down to the solution of Hamilton-Jacobi-Bellman partial differential equation. Compared with linear systems, the difficulty of nonlinear systems lies in that the HJB equation to be solved is often nonexistent or nonunique, which becomes the main obstacle to optimal control of nonlinear systems. This problem can be solved by introducing the inverse optimization into the design of uncertain nonlinear control systems through the robust control Lyapunov function [22]. The inverse optimization problem does not minimize the control law of a given target functional, but with the Lyapunov function for the robust stability of the system to make the controller is designed to minimize a backlog of objective functional, that is to say, first of all, get the control law, and then determine its optimal value function, so as to determine the optimal controller.

3.1. Derive the Control Law. For second order nonlinear systems,

$$\begin{aligned} \dot{x}_1 &= \phi(x_1) + x_2, \\ \dot{x}_2 &= u, \\ y &= x_1. \end{aligned} \tag{4}$$

(Step 1) For the subsystem x_1 in equation (4), virtual control law is designed with x_2 as the control input.

Choose the following form of control law:

$$x_2^{\text{des}} = -\psi(x_1). \tag{5}$$

Construct the following control Lyapunov function:

$$W(x_1) = \frac{1}{2}x_1^2. \tag{6}$$

Substituting into $x_2 = x_2^{\text{des}}$, its differential is $\dot{W} = (\phi(x_1) - \psi(x_1))x_1$.

When $(\phi(x_1) - \psi(x_1))x_1 < 0$ is satisfied, its negative definite can be guaranteed.

(Step 2) Introduce an error variable:

$$\bar{x}_2 = x_2 - x_2^{\text{des}} = x_2 + \psi(x_1). \tag{7}$$

So the system equation (4) is equal to

$$\begin{aligned} \dot{x}_1 &= \phi(x_1) - \psi(x_1) + \bar{x}_2, \\ \dot{\bar{x}}_2 &= u + \psi'(x_1)(\phi(x_1) - \psi(x_1) + \bar{x}_2). \end{aligned} \tag{8}$$

Construct the following control Lyapunov function:

$$V(x_1, \bar{x}_2) = F(x_1) + \frac{1}{2}\bar{x}_2^2, \tag{9}$$

where $F(x_1)$ is any effective control Lyapunov function of subsystem x_1, which means that when $x_2 = x_2^{des}$ is satisfied,

$$\dot{F}(x_1) = F'(x_1)(\phi(x_1) - \psi(x_1)) = -U(x_1), \tag{10}$$

where $U(x_1)$ is positive definite.

$$\begin{aligned} \dot{V} &= F'(x_1)[\phi(x_1) - \psi(x_1) + \bar{x}_2] + \bar{x}_2\left[u + \psi'(x_1)(\phi(x_1) - \psi(x_1) + \bar{x}_2)\right] \\ &= -U(x_1) + \bar{x}_2\left[F'(x_1) + u + \psi'(x_1)(\phi(x_1) - \psi(x_1)) + \psi'(x_1)\bar{x}_2\right). \end{aligned} \tag{11}$$

Choose $F'(x_1) = -\psi'(x_1)(\phi(x_1) - \psi(x_1))$, $F(0) = 0$; the item x_1 in the second items can be cancelled out.

Substituting $F'(x_1)$ into formula (10), the following formula can be obtained:

$$U(x_1) = \psi'(x_1)(\phi(x_1) - \psi(x_1))^2. \tag{12}$$

When $\psi'(x_1) > 0$ is satisfied, the positive definite is guaranteed.

And then, the Lyapunov function of the system is

$$\dot{V} = -U(x_1) + \bar{x}_2\left[u + \psi'(x_1)\bar{x}_2\right]. \tag{13}$$

In order to make $\dot{V}$ negative definite, the control law can be selected finally:

$$u = -k_2\bar{x}_2 = -k_2(x_2 + \psi(x_1)). \tag{14}$$

When $k_2 > \psi'(x_1)$ is satisfied, the negative definite of $\dot{V} = -U(x_1) - (k_2 - \psi'(x_1))\bar{x}_2^2$ is guaranteed.

3.2. Determine Its Optimal Value Function

Lemma 4 (see [23, 24]). *Consider the nonlinear system:*

$$\dot{x} = f(x) + g(x)u, \tag{15}$$

where $x \in R^n$ is the state variable and $u \in R^m$ is the control input.

And assume $g(x) \neq 0$. For a given feedback control $u(x)$, define the optimal value function:

$$J(x) = \int_0^\infty \left(Q(x) + u^T R(x) u\right) dt, \tag{16}$$

where $Q(x)$ is positive definite and $R(x)$ is symmetric positive definite.

The optimal value function $J(x)$ can be selected as the Lyapunov function $V(x)$. Then, the optimal control can be obtained:

$$u^*(x) = -\frac{1}{2} R^{-1}(x) \left(V_x(x) g(x)\right)^T. \tag{17}$$

Using Hamilton-Jacobi-Bellman equation

$$\min_u \left[Q(x) + u^T R(x) u + V_x(x)(f(x) + g(x)u)\right] = 0, \tag{18}$$

it can be obtained inversely:

$$\begin{aligned} R(x) &= -\frac{\left(V_x(x) g(x)\right)^T}{2u^*(x)}, \\ Q(x) &= -V_x(x) f(x) - \frac{1}{2} V_x(x) g(x) u^*(x). \end{aligned} \tag{19}$$

Based on Lemma 4, comparing the error system shown in equation (8) with the second order system shown in equation (4), the following can be obtained:

$$f(x) = \begin{pmatrix} \phi(x_1) - \psi(x_1) + \bar{x}_2 \\ \psi'(())(\phi(x_1) - \psi(x_1) + \bar{x}_2) \end{pmatrix}, g(x) = \begin{pmatrix} 0 \\ 1 \end{pmatrix}. \tag{20}$$

And

$$V_x = \left(F'(x_1)\bar{x}_2\right) = \left(-\psi'(x_1)(\phi(x_1) - \psi(x_1))\bar{x}_2\right). \tag{21}$$

Therefore, the optimal control performance parameters that can be achieved by the control law (17) are obtained by substituting formulas (20) and (21):

$$\begin{aligned} R(x) &= -\frac{\left(V_x(x) g(x)\right)^T}{2u(x)} = \frac{\bar{x}_2}{2k_2 \bar{x}_2} = \frac{1}{2k_2}, \\ Q(x) &= -V_x(x) f(x) - \frac{1}{2} V_x(x) g(x) u(x) \\ &= \psi'(x_1)(\phi(x_1) - \psi(x_1))^2 + \left(\frac{1}{2} k_2 - \psi'(x_1)\right) \bar{x}_2^2. \end{aligned} \tag{22}$$

If virtual control law $x_2^{des} = -\psi(x_1) = -k_1 x_1$ is selected, then, the linear control law of the system (4) is

$$u = -k_2(x_2 + k_1 x_1) \tag{23}$$

In order to $Q(x)$ be positive definite and the cost function to be a meaningful optimal performance, it must be guaranteed that

$$k_2 > 2k_1. \tag{24}$$

Therefore, combining (12), (14), and (23), we can get: when $0 < 2k_1 < k_2$ is satisfied; the origin of the system can be given global asymptotic stability.

And minimize the following optimal value function:

$$J = \int_0^\infty \left(\psi'(x_1)(\phi(x_1) - \psi(x_1))^2 + \left(\frac{1}{2}k - \psi'(x_1)\right)(x_2 + \psi(x_1))^2 + \frac{1}{2k} u^2\right) dt. \tag{25}$$

Similarly, if virtual control law $x_2^{des} = -\psi(x_1 - r) = -k_1 (x_1 - r)$ is selected, then, the linear control law of the system (4) is

$$\begin{aligned} u &= -k_2(\phi(r) + x_2 + k_1(x_1 - r)), \\ 0 &< 2k_1 < k_2. \end{aligned} \tag{26}$$

Defining $x - r = e$, the tracking problem of the system at $y = r$ can be transformed into the global asymptotic stability problem of the system at $x - r$, and the results of equations (23) and (24) above can be applied.

Then, the system obtains global asymptotic stability at $y = r$.

And minimize the following optimal value function:

$$\begin{aligned} J = \int_0^\infty \Bigg(& k_1 [\phi(x_1) - \phi(r) - k_1(x_1 - r)]^2 + \left(\frac{1}{2} k_2 - k_1\right) \\ & \cdot [x_2 + \phi(r) + k_1(x_1 - r)]^2 + \frac{1}{2k_2} u^2 \Bigg) dt. \end{aligned} \tag{27}$$

3.3. Design the Optimal Control Law. Considering the dynamics equation above, the following coordinate transformation is introduced:

$$\begin{bmatrix} p_d \\ q_d \\ r_d \end{bmatrix} = \begin{bmatrix} \cos\alpha \cos\beta & 0 & \sin\alpha \cos\beta \\ -\cos\alpha \sin\beta & \cos\beta & -\sin\alpha \sin\beta \\ -\sin\alpha & 0 & \cos\alpha \end{bmatrix} \begin{bmatrix} p \\ q \\ r \end{bmatrix}. \tag{28}$$

The corresponding dynamics equation becomes

$$\begin{bmatrix} \dot{\mu} \\ \dot{\alpha} \\ \dot{\beta} \end{bmatrix} = \begin{bmatrix} \frac{1}{\cos^2\beta} & 0 & 0 \\ 0 & \frac{1}{\cos\beta} & 0 \\ 0 & 0 & -1 \end{bmatrix} \begin{bmatrix} p_d \\ q_d \\ r_d \end{bmatrix} + \begin{bmatrix} F_\mu(X) \\ F_\alpha(X) \\ F_\beta(X) \end{bmatrix}. \tag{29}$$

Therefore, with the angular acceleration after coordinate transformation as the control input, a three-axis decoupled

second-order nonlinear system can be obtained, as shown below:

$$\begin{cases} \dot{\alpha} = \dfrac{1}{\cos\beta} \cdot q_d + F_\alpha(X), \\ \dot{q}_d = u_2, \end{cases} \tag{30}$$

$$\begin{cases} \dot{\beta} = -r_d + F_\beta(X), \\ \dot{r}_d = u_3, \end{cases} \tag{31}$$

$$\begin{cases} \dot{\mu} = \dfrac{1}{\cos^2\beta} \cdot p_d + F_\mu(X), \\ \dot{p}_d = u_1. \end{cases} \tag{32}$$

It can be found that the structures of equations (30), (31), (32), and (4) are exactly the same.

Comparing equations (4) and (30), the following can be found:

$$\begin{cases} x_1 = \alpha, \\ x_2 = \dfrac{1}{\cos\beta} \cdot q_d, \\ y = x_1, \end{cases} \quad \phi(x_1) = F_\alpha(X), \quad u = \frac{1}{\cos\beta} \cdot \dot{q}_d = \frac{1}{\cos\beta} \cdot u_2. \tag{33}$$

Therefore, it is easy to obtain the backstepping optimal controller to track control instructions $r = \alpha_{cmd}$:

$$u_2 = -k_q(q_d + \cos\beta F_\alpha(\alpha_{cmd}) + k_\alpha \cos\beta(\alpha - \alpha_{cmd})), \tag{34}$$

$$0 < 2k_\alpha < k_q. \tag{35}$$

At the same time, the following optimal value function can be minimized:

$$J = \int_0^\infty \left(k_\alpha[F_\alpha(\alpha) - F_\alpha(\alpha_{cmd}) - k_\alpha(\alpha\text{-}\alpha_{cmd})]^2 + \left(k_q - k_\alpha\right)\left[\frac{1}{\cos\beta} \cdot q_d + F_\alpha(\alpha_{cmd}) + k_\alpha(\alpha\text{-}\alpha_{cmd})\right]^2\right) dt. \tag{36}$$

Similarly, comparing equations (4) and (31), the following can be found:

$$\begin{cases} x_1 = \beta, \\ x_2 = -r_d, \\ y = x_1, \end{cases} \quad \phi(x_1) = F_\beta(X), \quad u = -\dot{r}_d = -u_3. \tag{37}$$

Therefore, it is easy to obtain the backstepping optimal controller to track control instructions $r = \beta_{cmd}$:

$$u_3 = k_r\left(-r_d + F_\beta(\beta_{cmd}) + k_\beta(\beta - \beta_{cmd})\right), \tag{38}$$

$$0 < 2k_\beta < k_r. \tag{39}$$

At the same time, the following optimal value function can be minimized:

$$J = \int_0^\infty \left(k_\beta\left[F_\beta(\beta) - F_\beta(()) - k_\beta(\beta - \beta_{cmd})\right]^2 + \left(k_r - k_\beta\right)\left[-r_d + F_\beta(\beta_{cmd}) + k_\beta(\beta - \beta_{cmd})\right]^2\right) dt. \tag{40}$$

Similarly, comparing equations (4) and (32), the following can be found:

$$\begin{cases} x_1 = \mu, \\ x_2 = \dfrac{1}{\cos^2\beta} \cdot p_d, \\ y = x_1, \end{cases} \quad \phi(x_1) = F_\mu(X), \quad u = \frac{1}{\cos^2\beta} \cdot \dot{p}_d = \frac{1}{\cos^2\beta} \cdot u_1. \tag{41}$$

Therefore, it is easy to obtain the backstepping optimal controller to track control instructions $r = \mu_{cmd}$:

$$u_1 = -k_p\left(p_d + \cos^2\beta F_\mu(\mu_{cmd}) + k_\mu \cos^2\beta(\mu - \mu_{cmd})\right), \tag{42}$$

$$0 < 2k_\mu < k_p. \tag{43}$$

At the same time, the following optimal value function can be minimized:

$$J = \int_0^\infty \left(k_\mu\left[F_\mu(\mu) - F_\mu(\mu_{cmd}) - k_\mu(\mu\text{-}\mu_{cmd})\right]^2 + \left(k_p - k_\mu\right)\left[\frac{1}{\cos^2\beta} \cdot p_d + F_\mu(\mu_{cmd}) + k_\mu(\mu\text{-}\mu_{cmd})\right]^2\right) dt. \tag{44}$$

Through formulas (34), (38), and (42), the angular acceleration $\omega_d'^{des} = [p'_{dcmd}\, q'_{dcmd}\, r'_{dcmd}]^T$ required to achieve attitude maneuver can be obtained. After integral operation and inverse coordinate transformation, the following formula can be obtained:

$$\omega^{des} = T_{bd}\left(\frac{1}{s}\omega_d'^{des}\right). \tag{45}$$

To this end, according to the expected flight attitude requirements, the angular velocity required to complete the maneuver can be obtained by using formula (45), and then,

through the following formula, it can be converted into the torque coefficient required by the maneuver, which is also the input of control allocation problem in the next section.

$$\begin{aligned} T &= IT_{bd}(\alpha, \beta)\dot{\omega}_d^{des} + \omega \times I\omega, \\ \nu &= (c_l c_m c_n)^T = \frac{1}{S\bar{q}} \text{ diag } (b, \bar{c}, b)^{-1} T, \end{aligned} \tag{46}$$

where T_{bd} is the coordinate transformation matrix converted to the body shafting, I is the rotational inertia matrix of the aircraft, b is the wingspan length, and $\bar{c}$ is the average aerodynamic chord length.

4. Fault Tolerant Control Design Based on Control Allocation

As mentioned above, as UAV plays an increasingly important role in the air combat system, the tasks it undertakes become more and more complex, and it needs to bear certain impact of faults. For the flight control system, the UAV has the characteristics of multicontrol surfaces, especially the introduction of multiredundant control surfaces, which provides a prerequisite for the reconfiguration control of UAV against actuator failures.

As shown in Figure 2, when the fault detection module in VMC finds that there is any fault mode toward actuators, the control allocation module in VMC will switch from the normal state to the specific fault state. Then, the fault tolerant control strategy based on the control allocation works, and the control instructions solved by the control allocation module will reflect the influence of the actuator fault mode.

4.1. Nonlinear Control Allocation Design Considerations. For the nonlinear system, assume its motion equation is

$$\dot{x} = f(x, g(x, u)), \tag{47}$$

where $f : R^n \times R^k \mapsto R^n$ and $g : R^n \times R^m \mapsto R^k$ are nonlinear and $k < m$.

It can be written as

$$\begin{aligned} \dot{x} &= f(x) + g_u(x, u), \\ g_u(x, u) &= B_v g(x, u), \end{aligned} \tag{48}$$

where $B_v \in R^{n \times k}$, f, and g have the same mapping form as above.

Introduce virtual controls:

$$\nu = g(x, u), \tag{49}$$

where $\nu \in R^k$; the state equation of the system can be rewritten as

$$\dot{x} = f(x) + B_v \nu = f(x) + B_v g(x, u). \tag{50}$$

Thus, nonlinear system (48) can be converted into equations (49) and (50), which can also use the standard form of the control allocation problem. It can be seen that with linear control allocation problem the difference is that mapping is a nonlinear form.

In the flight control system, the control allocation strategy is required to be solved in real time, but the nonlinear control allocation problem cannot be solved in real time. Therefore, one of the methods to solve this problem is to use the method of local approximation mapping, using linear mapping to approximate nonlinear mapping.

Through local Taylor form expansion, linearization at point u_0 can be obtained:

$$g(x, u) \approx g(x, u_0) + \frac{\partial g}{\partial u}(x, u_0) \cdot (u - u_0). \tag{51}$$

So introduce a linear mapping $B(x) = (\partial g / \partial u)(x, u_0)$; the nonlinear control allocation problem (49) can be converted to the linear control allocation problem:

$$\bar{\nu} = B(x)u, \tag{52}$$

$$\bar{\nu} = \nu - g(x, u_0) + B(x)u_0. \tag{53}$$

When a nonlinear control allocation problem is transformed into a linear problem, it can be solved in many ways. Optimization algorithms based on linear programming, with its lower operation cost and simplex method, have been widely studied in the process of solving control allocation problems [25, 26]. According to the authors' previous research results [27], the allocation algorithm based on linear programming is directly applied here.

Combined with formulas (52) and (53), the control allocation problem is described as follows.

For the known control efficiency matrix B and the given virtual control quantity $\nu(t)$, the feasible instruction $u(t)$ of the control surface is determined by considering the position limit and rate limit $\underline{u}(t) \le u(t) \le \bar{u}(t)$ of the control surfaces, so that $Bu(t) = \nu(t)$ is satisfied.

Thus, the linear programming problem can be solved with the following matrix:

$$\begin{aligned} A &= M \cdot B, b = -A \cdot u_{\min}, \\ Aeq &= [\,], beq = [\,], \\ f^T &= -\nu_d^T \cdot B, \\ lb &= 0 \; ub = u_{\max} - u_{\min}. \end{aligned} \tag{54}$$

The corresponding optimization objectives are

$$\max \left(\rho = \frac{\|B \cdot u\|}{\|\nu_d\|} \right) = \min \left(J = -\nu_d^T \cdot B \cdot u \right). \tag{55}$$

In the three-dimensional control allocation problem, the matrix M has only two rows, i.e.,

$$M = \begin{bmatrix} \nu_{d,2} & -\nu_{d,1} & 0 \\ \nu_{d,3} & 0 & -\nu_{d,1} \end{bmatrix} \tag{56}$$

and the coefficient matrix $A = M \cdot B$ of constraint conditions

also has only two rows, whose rank is 2. Therefore, the solution process is relatively simple.

The application of the method in the flight control system is toward to $v = (c_l\, c_m\, c_n)^T = (1/S\bar{q})\ \mathrm{diag}\,(b, \bar{c}, b)^{-1} T$, and the specific process can be summarized as the following steps:

(Step 1) According to the theory of nonlinear control allocation, the control efficiency matrix under nonlinear condition should be calculated from the expression of aerodynamic derivative $C_M = (C_l\, C_m\, C_n)^T$:

$$B(x) = \frac{\partial C_M}{\partial \delta}(\alpha, \beta, p, q, r, \delta_0). \tag{57}$$

δ_0 can be selected as the control input $u(t - T)$ of previous sampling time or a fixed point, such as $\delta_0 = 0$.

(Step 2) Then the virtual control input after Taylor linear expansion is calculated:

$$\bar{v} = v - C_M(\alpha, \beta, p, q, r, \delta_0) + B(x)\delta_0. \tag{58}$$

(Step 3) Using the control allocation method of formula (54) to solve the above formula, the solution of formula (58) can be obtained.

4.2. Fault Tolerant Control Design for Actuators. This section describes the fault-tolerant control scheme according to the control allocation design method described in Section 4.1 for the two possible fault modes of the electric actuators described in Figure 1. Fault mode 1 is nonoutput force of the actuator, and the other fault mode is output shaft stuck of the actuator.

The nonlinear system equations of an aircraft under normal conditions are described as follows:

$$\dot{x} = f(x) + B_v v = f(x) + B_v g(x, u), \tag{59}$$

where $g(x, u)$ represents the control efficiency of surfaces, which will change when the surfaces fails due to actuators. The following equation describes the nonlinear system equation of the aircraft in the case of failure:

$$\dot{x} = f(x) + B_v g_f(x, u_f), \tag{60}$$

where $g_f(x, u_f)$ represents the control efficiency matrix in the case of failure and $u_f \in R^n$ represents the control input. For different fault modes, equation (60) corresponds to different function forms.

According to the requirements of reconfiguration control, control allocation needs to achieve:

$$g(x, u) = g_f(x, u_f). \tag{61}$$

For the control allocation problem under normal conditions, the allocation objective is

$$v(t) = g(x, u). \tag{62}$$

The nonlinear control allocation problem (62) can be converted to the linear control allocation problem:

$$\bar{v} = v - g(x, u_0) + B(x)u_0 = B(x)u. \tag{63}$$

Similarly, for the control allocation problem under faulty conditions, the allocation objective is

$$v_f(t) = g_f(x, u_f). \tag{64}$$

After linearization,

$$g_f(x, u_f) \approx g_f(x, u_0) + \frac{\partial g_f}{\partial u}(x, u_0) \cdot (u_f - u_0). \tag{65}$$

The control efficiency matrix $B_f(x) = (\partial g_f/\partial u)(x, u_0)$ is introduced, and the linear control allocation problem similarly is as follows:

$$\bar{v}_f = v_f - g_f(x, u_0) + B_f(x)u_0 = B_f(x)u. \tag{66}$$

When the fault modes of the actuators occur, the change of aerodynamic coefficient, weight, and center of gravity of the aircraft can be ignored. On this premise, the change of control capability caused by the faulty actuators only comes from the change of control input.

Meanwhile, when the linearized equilibrium points are $u_0 = 0$, the following formula can be obtained:

$$g(x, u_0) = g_f(x, u_0), \tag{67}$$

$$B(x)u_0 = B_f(x)u_0. \tag{68}$$

Thus, compare formulas (64) and (67), and the requirements of reconfiguration control (61) can be converted into

$$\bar{v}(t) = \bar{v}_f(t). \tag{69}$$

4.2.1. Fault Mode 1: Output Shaft Stuck. The output shaft stuck of actuator refers to the fault mode in which the actuator is in a fixed position due to motor blocking or other mechanical reasons, which can be realized by the fault detection module of VMC. In this fault mode, the control surface connected to the actuator will also be stuck in a certain position. In this case, its deflection will not only fail to produce the desired control effect but also to produce unwanted additional forces and unwanted additional torques. Therefore,

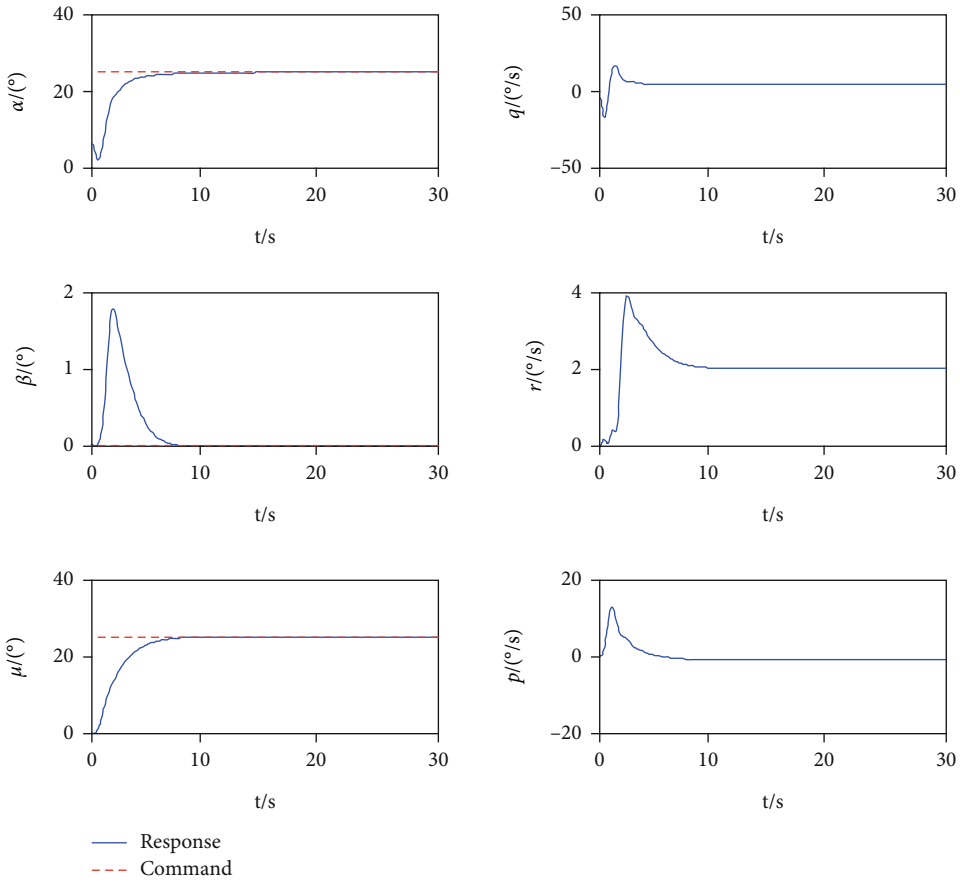

Figure 3: The state response of three-axis maneuver.

the influence of the stuck actuator must be offset in the control allocation.

When the shaft of actuator is stuck, the motion equation of the aircraft does not change, as shown in equation (60).

According to formula (66), the solution of control allocation for reconstruction control can be obtained:

$$\bar{v} = Bu = B_f u_f = B_f^* \cdot u_f^* + b_j \delta_f, \tag{70}$$

where assuming that the aircraft has m surfaces, $u_f^* = (\delta_1, \delta_2, \cdots \delta_j \cdots \delta_{m-1}) \in R^{m-1}$, B_f^* is the remaining control efficiency matrix after removing the stuck surface in B_f, b_j is the control efficiency coefficient of the stuck surface, and δ_f is the stuck position of the faulty surface.

After further derivation, the following can be obtained:

$$u_f^* = \left(B_f^*\right)^+ Bu - \left(B_f^*\right)^+ b_j \delta_f \tag{71}$$

Among them, the first item redistributes the torque required by the original surface to the remaining effective surfaces, and the second item is used to offset the additional influence caused by the stuck surface, so that the actual output of the stuck rudder surface is

$$u_f = \left(\delta_1, \delta_2, \cdots, \delta_{j-1}, \delta_f, \delta_{j+1}, \cdots, \delta_{m-1}\right). \tag{72}$$

4.2.2. Fault Mode 2: Nonoutput Force. Nonoutput force of actuator refers to the failure mode in which the clutch cuts off the current control output due to various reasons, and then, the actuator has no output force. It can be realized by the fault detection module of VMC. In this fault mode, the surface connected with the actuator will also be in a loosely floating state, that is, the control efficiency of the surface is zero. Then, it can be assumed that the loosely floating surface will not produce any aerodynamic and aerodynamic torque; that is, the effect of the control surface on the control input of the aircraft is zero.

Similar to fault mode 1, when the actuator has no output force, the state equation of the aircraft does not change. That is, only the control input of the loosely floating surface is zero, and the loss of control capability caused by the loss of control capability needs to be compensated by the remaining effective control surfaces.

Similarly, assuming u_f^* is the input of the remaining surface after removing the loosely-floating one, then,

$$\bar{v} = Bu = B_f u_f = B_f^* \cdot u_f^* + b_j \delta_f, \tag{73}$$

where, assuming that the aircraft has m surfaces, $u_f^* = (\delta_1, \delta_2, \cdots \delta_j \cdots \delta_{m-1}) \in R^{m-1}$, B_f^* is the remaining control efficiency matrix after removing the loosely floating surface in

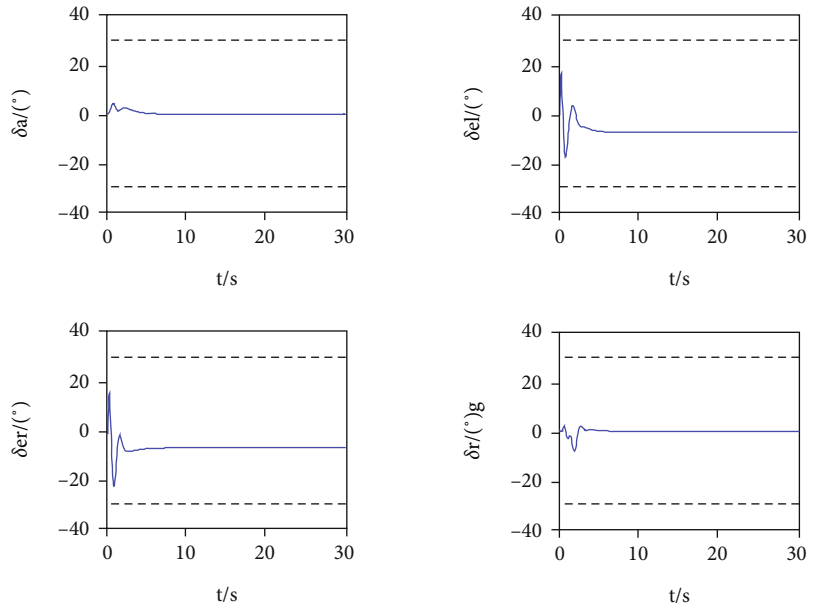

Figure 4: The deflection angle of surfaces. The forces and torques created by the four independent surfaces contribute to the aircraft's three-axis maneuver.

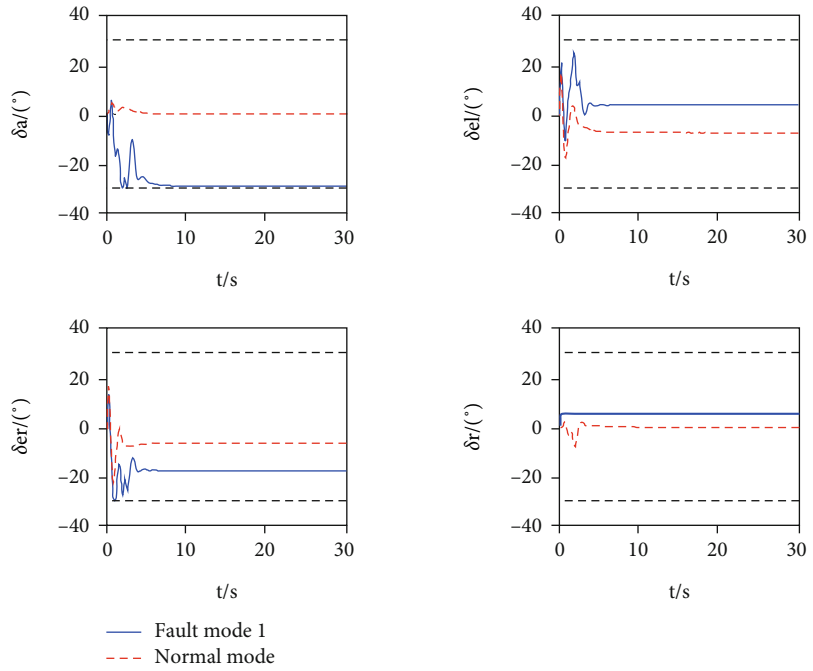

Figure 5: The deflection angle of surfaces against fault mode 1. The remaining surfaces compensate for the abnormal forces and torques caused by the stuck actuator attached to rudder.

B_f, b_j is the control efficiency coefficient of the loosely-floating surface, and $\delta_f = 0$.

Further derivation can be obtained:

$$u_f^* = \left(B_f^*\right)^+ Bu - \left(B_f^*\right)^+ b_j \delta_f. \tag{74}$$

Then, the actual output of the surfaces when the actuator has no output force can be obtained:

$$u_f = \left(\delta_1, \delta_2, \cdots \delta_{j-1}, 0, \delta_{j+1}, \cdots \delta_{m-1}\right). \tag{75}$$

5. Numerical Simulation

5.1. Control Objective. Based on the design of backstepping optimal controller in Section 3 and fault-tolerant control based on control allocation in Section 4, numerical simulations are conducted for the UAV.

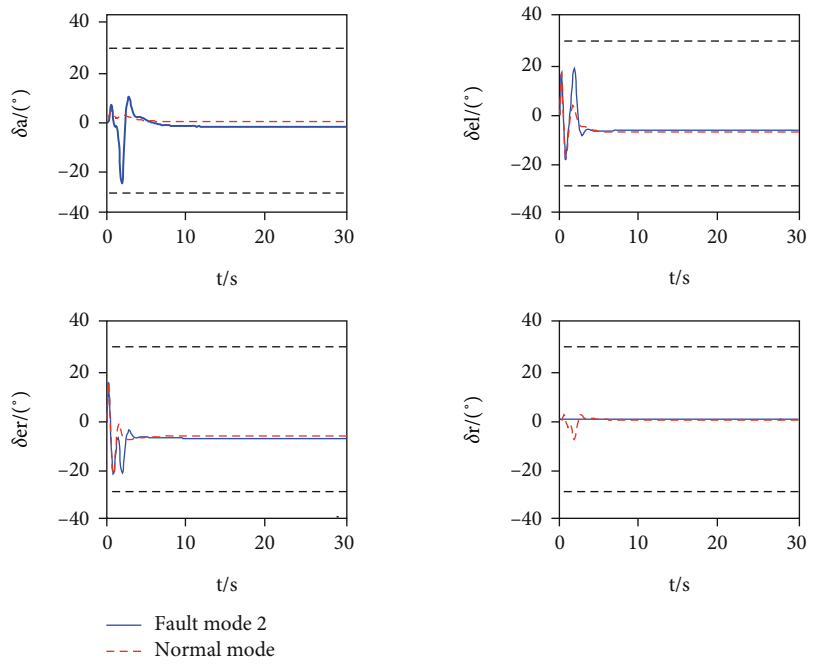

Figure 6: The deflection angle of surfaces against fault mode 2. The remaining surfaces also compensate for the loss forces and torques caused by the loosely floating actuator attached to rudder.

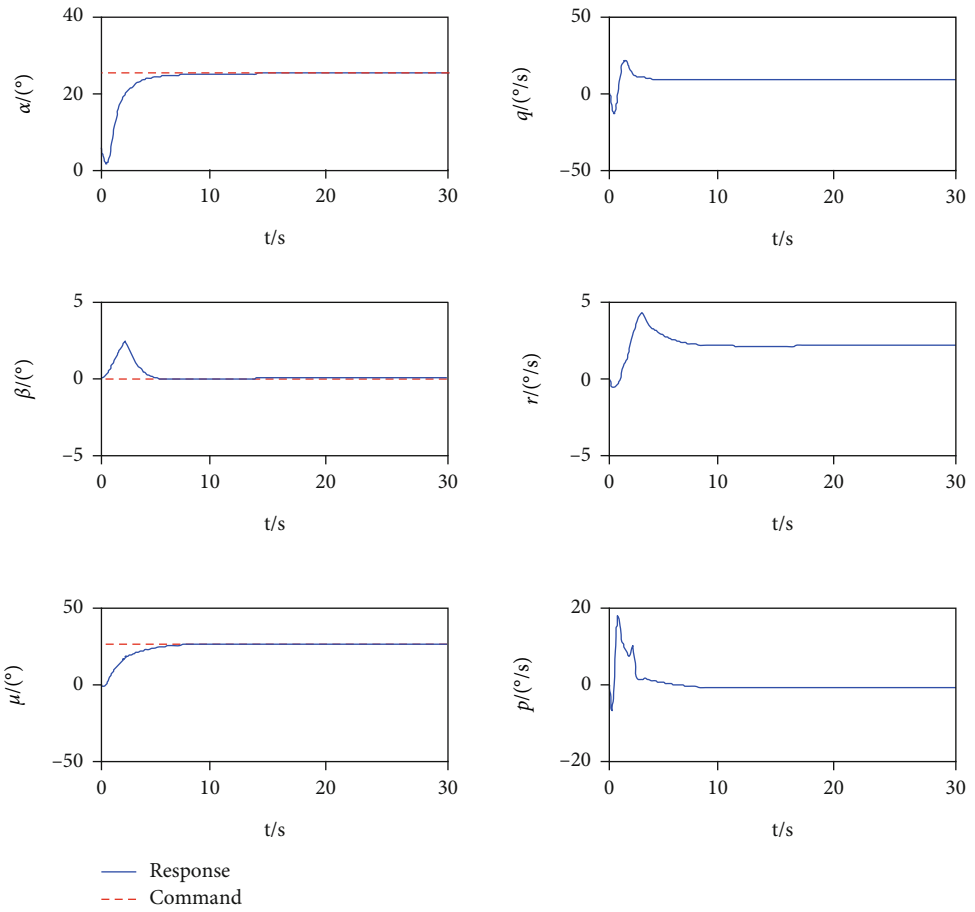

Figure 7: The state response of three-axis maneuver against fault mode 1.

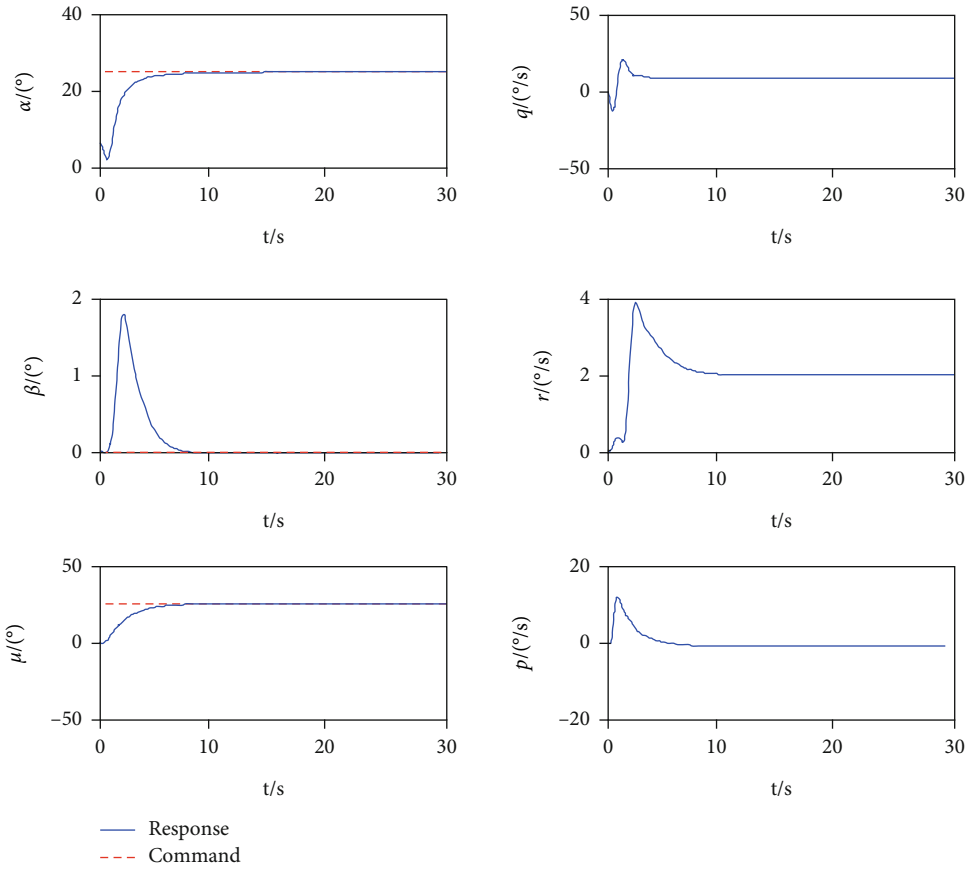

Figure 8: The state response of three-axis maneuver against fault mode 2.

In order to prove the correctness of the control law, the numerical simulation is carried out under the comparison of the two cases. The first set is three-axis maneuver without actuator failures, and the control objectives are $\alpha_{cmd} = 25^\circ$, $\beta_{cmd} = 0^\circ$, $\mu_{cmd} = 25^\circ$.

The fault tolerant control of three-axis maneuver under the condition of actuator faults is the second set. As above, the same simulated UAV object is used, and the initial trim conditions are the same. In the simulation, the parameters of backstepping optimal control law do not change, but the allocation algorithm switches from normal modes to the fault modes in control allocation. Also consider the three-axis maneuver; the control objectives are $\alpha_{cmd} = 25^\circ$, $\beta_{cmd} = 0^\circ$, $\mu_{cmd} = 25^\circ$.

Firstly, the deflection characteristics of the four surfaces of the UAV, namely, left elevator, right elevator, aileron, and rudder, are limited as follows:

$$U_{\max} = [30^\circ, 30^\circ, 30^\circ, 30^\circ],$$
$$U_{\min} = [-30^\circ, -30^\circ, -30^\circ, -30^\circ]. \quad (76)$$

It should be added here that the surface is stuck beyond the deflection limit due to mechanical reasons, and VMC cannot give the correct diagnosis through the fault detection module. The control allocation method may invalidate the input saturation strategy in these fault modes. And this failure condition is not covered in the paper because it cannot be correctly diagnosed.

Then, the initial trim conditions of the simulation are shown below: the trimming velocity is $V = 350$ft/s, the trimming angle of attack is $\alpha_0 = 6.76^\circ$, the remaining trimming flight statuses are $\beta_0 = \mu_0 = p_0 = q_0 = r_0 = 0$, and the trimming angles of deflection are, respectively $[\delta_{el}, \delta_{el}, \delta_a, \delta_r] = [-0.4449^\circ, -0.4449^\circ, -1.6193^\circ, 0.3226^\circ]$.

Finally, the parameters of the optimal controller described in Section 3 are $k_\alpha = 2.53$, $k_q = 5.76$, $k_\beta = 1.36$, $k_r = 5.14$, $k_\mu = 1.64$, and $k_p = 6.23$.

5.2. Simulation Result. It can be seen from the simulation results that the backstepping optimal controller can achieve a good control effect. In the control channels of the three axes, the controlled quantity can meet the requirements of the control instruction within 5 s, and the response has no overshoot and no steady-state error, refer to Figure 3. The black dotted lines in Figure 4 are the upper and lower limits of surface deflection. This proves that it is feasible and correct to design flight control system using backstepping optimal controller. At the same time, it also shows that the control allocation method can realize the correct distribution of control instructions on each controllable surface.

5.3. Simulation of Fault Mode 1. In the simulation, the electric actuator attached to the rudder is set to be stuck at 5°. Then, the rudder will also be stuck at 5°, and its deflection

will fail not only to produce the desired control effect but also to produce unwanted control effect.

5.4. Simulation of Fault Mode 2. In the simulation, the electric actuator attached to the rudder is set to nonoutput force. Then, the rudder will also be in a loosely floating state. Then, it can be assumed that the loosely floating rudder will not produce any aerodynamic and aerodynamic torque.

In Figures 5 and 6, the red curve is the deflection angle of surfaces without the actuator failure, and the blue curve is the deflection angle of surfaces in the corresponding fault mode, and the black dotted lines are the upper and lower limits of surface deflection. It can be seen that when actuator failures occur, the reconfiguration based on the control allocation method ensures remaining surfaces can compensate the influence caused by the faulty actuator. The angle of attack and the angle of roll track the control objectives quickly with stable performance; refer to Figures 7 and 8. Therefore, the design of control allocation completes the task of reconfiguration control well, obtains good control effect, and achieves the goal of fault-tolerant control.

6. Conclusion

The fault-tolerant control of UAV in the case of actuator failure in the flight control system is studied. Based on the backstepping control method derived from Lyapunov function, the nonlinear optimal control law was constructed by introducing inverse optimization strategy. And reconfiguration design based on control allocation is proposed. Through linearized nonlinear mapping, a fault-tolerant control scheme is designed for the actuators in two typical fault modes: stuck and nonoutput force. Through rigorous mathematical analysis and numerical simulation, the effectiveness of the control strategy is verified.

The integrated VMC in the FCS can realize online monitor of limited fault modes of actuators, which ensures the scheme proposed achieves better fault-tolerant control after the occurrence of known fault modes. However, mechanical transmission from the actuators to the surfaces, or the surfaces itself, cannot be directly dealt with by using the strategy proposed in the paper due to the lack of monitor results, such as the loss of part of the surface. It is worth further study.

Data Availability

No data were used to support to this study.

Conflicts of Interest

The authors declare that there are no conflicts of interest regarding publication of this article.

Acknowledgments

This work is cosupported by the Aeronautical Science Foundation of China (201958053003) and (20200007018001).

References

[1] H. Yin, J. Fan, T. Hou, D. Li, Y. Wang, and H. Chen, "Efficiency analysis of typical application based on manned/unmanned aerial vehicle cooperative combat," in *Proceedings of 2020 3rd International Conference on Unmanned Systems*, pp. 314–319, Harbin, China, 2020.

[2] L. Lei, "Development analysis of typical manned/unmanned aerial vehicle collaborative operations projects abroad," *Unmanned Systems Technology*, vol. 3, no. 4, pp. 83–90, 2020.

[3] L. Yue, H. Wei, and W. Yongqing, "Deep reinforcement learning with application to air confrontation intelligent decision-making of manned/unmanned aerial vehicle cooperative system," *IEEE Access*, vol. 8, pp. 67887–67898, 2020.

[4] P. M. Frank, "Fault diagnosis in dynamic systems using analytical and knowledge-based redundancy: a survey and some new results," *Automatica*, vol. 26, no. 3, pp. 459–474, 1990.

[5] Z. Zejun, Y. Hao, and J. Bin, "Fault tolerant consensus of multiple nonholonomic chained-form systems with actuator and communication faults," *International Journal of Robust and Nonlinear Control*, vol. 31, no. 18, pp. 9483–9500, 2021.

[6] M. Taimoor and L. Aijun, "Neural-sliding mode approach-based adaptive estimation, isolation and tolerance of aircraft sensor fault," *Aircraft Engineering and Aerospace Technology*, vol. 92, no. 2, pp. 237–255, 2019.

[7] J. Marzat, D. F. Piet-Lahanier, F. Damongeot, and E. Walter, "Model-based fault diagnosis for aerospace systems: a survey," *Proceedings of the Institution of Mechanical Engineers, Part G: Journal of Aerospace Engineering*, vol. 226, no. 10, pp. 1329–1360, 2012.

[8] J. Hu and X. Lingfei, "Multi-sensor fault diagnosis of aircraft engine based on Kalman Filter Group," *Proceedings of 2016 Chinese Intelligent Systems Conference*, vol. 404, pp. 363–379, 2016.

[9] Y. Gao, N. Wenhui, and F. Wan, "Deep belief net-based fault diagnosis of flight control system sensors," *Journal of Physics: Conference Series*, vol. 1631, no. 1, article 012186, 2020.

[10] I. Samy, I. Postlethwaite, and D.-W. Gu, "Survey and application of sensor fault detection and isolation schemes," *Control Engineering Practice*, vol. 19, no. 7, pp. 658–674, 2011.

[11] Y. Baojun and S. Zhaorui, "Reconfiguration of the angle of attack signal in disability of sensors," *Aeronautical Science & Technology*, vol. 29, no. 8, pp. 33–40, 2018.

[12] Y. Jun, N. Jing, and G. Guanbin, "Robust model reference adaptive control for transient performance enhancement," *International Journal of Robust and Nonlinear Control*, vol. 30, no. 15, pp. 6207–6228, 2020.

[13] R. B. Anderson, J. A. Marshall, A. L'Afflitto, and J. M. Dotterweich, "Model reference adaptive control of switched dynamical systems with applications to aerial robotics," *Journal of Intelligent and Robotic Systems*, vol. 100, no. 3-4, pp. 1265–1281, 2020.

[14] K. Prasanth, E. Ryan, and S. Koushil, "Geometric L1 adaptive attitude control for a quadrotor unmanned aerial vehicle," *Journal of Dynamic Systems, Measurement, and Control*, vol. 142, no. 3, article 031003, 2020.

[15] L. Yuqian, C. Jiaxing, and C. Chengyu, "Advanced autonomous underwater vehicles attitude control with L1 backstepping adaptive control strategy," *Sensors*, vol. 19, no. 22, article 4848, 2019.

[16] Z. Youmin and J. Jin, "Fault tolerant control system design with explicit consideration of performance degradation," *IEEE*

Transactions on Aerospace and Electronic Systems, vol. 39, no. 3, pp. 838–848, 2003.

[17] C. Yuwei, Z. Zhengyong, L. Zhengren, and L. Aijun, "A task scheduling method for network distributed flight control system," in *2019 Chinese Automation Congress, CAC*, pp. 480–483, Hangzhou, China, 2019.

[18] X. Wang, H. Fang, L. Dou, B. Xin, and J. Chen, "Integrated distributed formation flight control with aerodynamic constraints on attitude and control surfaces," *Nonlinear Dynamics*, vol. 91, no. 4, pp. 2331–2345, 2018.

[19] C. Yuwei and L. Aijun, "Research on the key technologies of network distributed flight control system," in *2020 Chinese Automation Congress, CAC*, pp. 6928–6931, Shanghai, China, 2020.

[20] S. Marc and P. Anthony, "Nonlinear adaptive flight control with a backstepping design approach," in *AIAA Guidance, Navigation, and Controsl Conference and Exhibit*, pp. 728–738, Boston, M A, U.S.A., 1998.

[21] H. Kaiyu, Y. Aaly, and C. Zian, "Fuzzy adaptive backstepping control of nonlinear uncertain systems with unmeasured states and input saturation," *IEEE Access*, vol. 8, pp. 228442–228453, 2020.

[22] J. Lofberg, "Backstepping with local LQ performance and global approximation of quadratic performance," in *Proceedings of the 2000 American Control Conference*, vol. 6, pp. 3898–3902, Chicago, IL, USA, 2000.

[23] S. Kang, J. Back, H. Shim, and J. H. Seo, "Locally optimal and robust backstepping design for C1 vector fields," in *International Conference on Control, Automation and Systems*, pp. 2212–2217, Seoul, Korea (South), 2007.

[24] K. Ezal, Z. Pan, and P. V. Kokotovic, "Locally optimal and robust backstepping design," *IEEE Transactions on Automatic Control*, vol. 45, no. 2, pp. 260–271, 2000.

[25] H. Xiuwei and D. Guangren, "Dynamic infinity-norm constrained control allocation for attitude tracking control of overactuated combined spacecraft," *IET Control Theory and Applications*, vol. 13, no. 11, pp. 1692–1703, 2019.

[26] Y. Wen, L. Chen, K. Liang, and D. Duan, "Nonlinear MPC for a sensorless multi-vectored propeller airship based on sliding mode observer with saturation," *Asian Journal of Control*, vol. 21, no. 1, pp. 248–263, 2019.

[27] Y. W. Cui, W. G. Zhang, G. W. Li, and J. P. Shi, "Research for multi-control-effector reconfigurable control based on linear programming," *Flight Dynamics*, vol. 29, no. 2, pp. 41–45, 2011.